

Toponium: the smallest bound state and simplest hadron in quantum mechanics

Jing-Hang Fu,^{1,*} Yu-Ji Li,^{2,*} Hui-Min Yang,³ Yu-Bo Li,⁴ Yu-Jie Zhang,^{1,5,†} and Cheng-Ping Shen^{6,7,‡}

¹*School of Physics, Beihang University, Beijing 100083, China.*

²*Institute of Modern Physics, Fudan University, Shanghai, China.*

³*Center of High Energy Physics, Peking University, Beijing, China.*

⁴*School of Physics, Xi'an Jiaotong University, Xi'an, China.*

⁵*Peng Huanwu Collaborative Center for Research and Education, Beihang University, Beijing 100191, China.*

⁶*Key Laboratory of Nuclear Physics and Ion-beam Application (MOE) and
Institute of Modern Physics, Fudan University, Shanghai 200443, China.*

⁷*School of Physics, Zhengzhou University, Zhengzhou 450001, China*

We explore toponium, the smallest known quantum bound state of a top quark and its antiparticle, bound by the strong force. With a Bohr radius of 8×10^{-18} m and a lifetime of 2.5×10^{-25} s, toponium uniquely probes microphysics. Unlike all other hadrons, it is governed by ultraviolet freedom. This distinction offers novel insights into quantum chromodynamics. Our analysis reveals a toponium signal exceeding 5σ in the distribution of the cross section ratio between $e^+e^- \rightarrow b\bar{b}$ and $e^+e^- \rightarrow q\bar{q}$ ($q = b, c, s, d, u$), based on 400 fb^{-1} of data collected at $\sqrt{s} \approx 341$ GeV. This discovery enables a top quark mass measurement with an uncertainty reduced by a factor of ten compared to current precision levels. Moreover, this method improves the systematic uncertainty by at least a factor of 12 compared to any other possible methods.

Introduction—The top quark (t), the heaviest known element particle, plays a pivotal role in Standard Model (SM) of particle physics. Its unique properties, particularly its mass, have far-reaching implications for our understanding of fundamental forces and the stability of the universe. Toponium, a bound state of a top quark and an anti-top quark (\bar{t}), represents the smallest quantum mechanical bound state known to date. Formed by strong force, toponium has nearly twice the mass of a single top quark [1, 2]. With the smallest Bohr radius of 8×10^{-18} m and an extremely short lifetime of 2.5×10^{-25} s, the study of toponium offers a unique opportunity to explore fundamental aspects of quantum mechanics, including entanglement [3–6], as well as to explore quantum gravity and extra dimensions [7, 8] at scales of 10^{-18} m and 10^{-25} s.

The top quark mass (m_t) is a crucial fundamental parameter in SM, as m_t significantly influences our understanding of SM, particularly its vacuum stability, and provides a window into potential new physics beyond SM [9–12]. Despite its importance, m_t cannot be predicted theoretically and must be measured experimentally. The most precise measurement to date [2] yields an on-shell mass of $m_t^{\text{OS}} = (172.52 \pm 0.14_{\text{stat.}} \pm 0.30_{\text{syst.}}) \text{ GeV} = (172.52 \pm 0.33) \text{ GeV}$. While the statistical uncertainty (stat.) can be reduced with longer data acquisition time, the systematic uncertainty (syst.) defines the ultimate precision of the measurement.

The most precise method for determining m_t involves the near-threshold production of $t\bar{t}$ at future electron positron (e^+e^-) colliders, such as the Circular Electron Positron Collider (CEPC) [13, 14] and the Future Circular Lepton Collider (FCC-ee) [15]. Projections suggest that m_t could be measured to a precision of 25 – 59 MeV

at CEPC [16] and 40 – 75 MeV at FCC-ee [17], with statistical uncertainties as low as 9 MeV at integrated luminosities of 100 – 200 fb^{-1} around 343 GeV, although systematic uncertainties will dominate. These uncertainties arise from multiple sources, such as beam energy calibration, theoretical modeling, and detector performance [16, 18]. Therefore, the accurate determination of m_t relies heavily on the development of novel method and advanced systematic control.

Despite the challenges, precise measurement of m_t is essential for refining theoretical models such as supersymmetry and two Higgs doublet models, allowing tighter constraints on their parameter spaces [19, 20]. Furthermore, these precise m_t determinations have far-reaching implications for cosmology and fundamental physics [21], and the source of inflation in the universe [22], making them indispensable for current and future research. The coupling between t and the Higgs boson (H), which generates m_t , is one of the strongest fundamental interactions, remaining significant - second only to gravity - and potentially constraining the safety of quantum gravity at energy scales far beyond the Planck scale (10^{19} GeV) [23].

In addition to the on-shell top quark mass m_t^{OS} and other scheme- and model-dependent definitions, the 1S mass of top quark, defined as $m_t^{1\text{S}} = m_{J_t}/2$ (where J_t denotes the spin-triplet ground state of toponium) [24], constitutes the sole scheme- and model-independent measure of the top quark mass m_t [25–27].

Furthermore, toponium distinguishes itself among hadrons because its behavior is governed by ultraviolet freedom, rather than infrared slavery of quantum chromodynamics (QCD) at distances of roughly 200 MeV [28, 29]. This unique characteristic enables

toponium to be theoretically described by perturbative QCD (PQCD), thereby offering new insights into confinement within QCD [28]. Given its high binding energy, the phase transition between toponium and free top quark pairs could have profound implications for the structure of the quark-gluon plasma [30], cooling rates [31], and the supercooled electroweak phase transition in the early universe [32–34].

In this Letter, we propose a method to discover J_t and accurately determine m_t^{IS} by measuring the cross section ratio:

$$R_b = \frac{\sigma_{\text{Born}}(e^+e^- \rightarrow b\bar{b})}{\sum_{q=u,d,s,c,b} \sigma_{\text{Born}}(e^+e^- \rightarrow q\bar{q})} \quad (1)$$

at e^+e^- colliders near $2m_t^{\text{IS}}$, where b is the bottom quark and q is a quark for $u, d, s, c, \text{ or } b$. Future measurements of R_b at the Z pole are expected to achieve precision levels of 4×10^{-5} at CEPC [13] and less than 6×10^{-5} at FCC-ee [35]. The relative precision of R_b at 365 GeV with 1.5 ab^{-1} data will be 9.6×10^{-4} at FCC-ee [36], which results an absolute precision level of 1.4×10^{-4} . The other possible methods to identify toponium can be found in Refs. [37–39] and related papers.

Modeling J_t Interaction—We introduce the Lagrangian density \mathcal{L}_{J_t} of the field J_t into that of SM, \mathcal{L}_{SM} [37] as follows:

$$\mathcal{L}_{J_t} = \sum_{f=b,e} \bar{f} \left(g_{J_t f f}^V \gamma_\mu + g_{J_t f f}^A \gamma_\mu \gamma^5 \right) f J_t^\mu + \dots \quad (2)$$

where the coupling factors $g_{J_t f f}^V$ and $g_{J_t f f}^A$ are determined by non-relativistic QCD (NRQCD) [40], f represents the field of either the b quark or the electron, and J_t^μ is the field of J_t .

The J_t bound state is obtained by the Schrödinger equation with the Coulomb potential between t and \bar{t} as a lattice QCD result at an infinite quark mass [41, 42],

$$V(r) = -\frac{\lambda}{r}. \quad (3)$$

The Coulombic coefficient $\lambda = 0.285 \pm 0.011$ [41, 42], and r is the distance between t and \bar{t} . We derive the binding energy B_{J_t} , mass $m_{J_t} = 2m_t^{\text{OS}} - B_{J_t} = 2m_t^{\text{IS}}$, and the square of the wave function at the origin $|\psi_{J_t}(0)|^2$:

$$\begin{aligned} B_{J_t} &= \frac{\lambda^2 m_t^{\text{OS}}}{4} = (3.503 \pm 0.270) \text{ GeV}, \\ m_{J_t} &= (341.537 \pm 0.653_{m_t^{\text{OS}}} \pm 0.270_\lambda) \text{ GeV} \\ &= (341.537 \pm 0.707) \text{ GeV}, \\ |\psi_{J_t}(0)|^2 &= \frac{(\lambda m_t^{\text{OS}})^3}{8\pi}. \end{aligned} \quad (4)$$

The uncertainty in m_{J_t} is mainly due to m_t^{OS} . The Bohr radius of toponium is calculated to be $8 \times 10^{-18} \text{ m}$.

The B_{J_t} and $|\psi_{J_t}(0)|^2$ have also been calculated in PQCD, but the convergence of the perturbative series up to next-to-next-to-next-to-leading order (NNNLO) is still unsatisfactory (End Matter), requiring the consideration of higher order corrections. Including the Higgs and photon contributions [43], the NNNLO binding energy is 3.194 GeV, which is comparable to the B_{J_t} in Eq.(4). The estimated production cross section of spin-singlet toponium at the Large Hadron Collider (LHC) at 13 TeV, assuming identical masses and wave functions for the toponium states, is 6.24 pb. This estimate agrees with the value of 6.43 pb reported in Refs. [37, 38] and the recent CMS result of $(7.1 \pm 0.8) \text{ pb}$ [44].

The width Γ_{J_t} of J_t is dominated by twice the width of the top quark Γ_t [45, 46]:

$$\Gamma_{J_t} = 2\Gamma_t \left(1 - \frac{\lambda^2}{8} \right) + \Gamma_{\text{Anni}} = (2.603 \pm 0.019) \text{ GeV} \quad (5)$$

where the coefficient $(1 - \lambda^2/8)$ comes from corrections for the fact that bound top quarks are different from free top quarks [47]. The annihilation decay width of J_t , $\Gamma_{\text{Anni}} = 0.0093 \text{ GeV}$, is calculated using NRQCD [40].

With the Breit-Wigner formula [48], the Feynman amplitude of the J_t medium particle is:

$$\mathcal{M}(J_t) \propto \frac{\lambda^3}{s - m_{J_t}^2 + i\Gamma_{J_t} m_{J_t}}, \quad (6)$$

where m_{J_t} and Γ_{J_t} are its mass and width, λ^3 is part of the coupling factors $g_{J_t f f}^V$ and $g_{J_t f f}^A$, and \sqrt{s} is the center of mass energy. The real part of the denominator $s - m_{J_t}^2$ goes from negative to 0 to positive as \sqrt{s} goes over m_{J_t} . In the amplitudes $\mathcal{M}(\gamma)$ and $\mathcal{M}(Z)$ corresponding to the contributions of the photon (with $m_\gamma = \Gamma_\gamma = 0$) and the Z boson (with $m_Z = 91.188 \text{ GeV}$) in SM respectively, the sign of the term $s - m^2$ remains unaltered. This results in a characteristic dip-bump structure in the R_b distribution, stemming from the fact that the production probabilities for quantum interference are proportional to the square of the sum of amplitudes, namely $|\mathcal{M}(J_t) + \mathcal{M}(\gamma) + \mathcal{M}(Z)|^2$. This dip-bump structure in the R_b distribution of SM with J_t is seen in Fig. 1, while the R_b distribution of SM without J_t is very close to a horizontal straight line. By observing the deviation of R_b distribution from the straight line, we can identify J_t , and a precise measurement of this deviation allows us to determine m_t^{IS} .

We choose the central values of m_{J_t} and λ as input, and our results will demonstrate the validity of this method within the corresponding ranges. Since Γ_{J_t} can be predicted within a certain range in SM without affecting our conclusions, we fix Γ_{J_t} to its central value.

Measuring R_b —The R_b , an observable which can be precisely measured in a pseudo-experiment with the

CEPC scenario, is obtained by [49] (End Matter):

$$R_b = \frac{N_{\text{tag}} F_{\text{hadron}}^{udsc} - N_{\text{hadron}} F_{\text{tag}}^{udsc}}{N_{\text{tag}} (F_{\text{hadron}}^{udsc} - F_{\text{hadron}}^b) + N_{\text{hadron}} (F_{\text{tag}}^b - F_{\text{tag}}^{udsc})}. \quad (7)$$

Here, $F = \varepsilon f_{\text{ISR}}$, the detection efficiency for b quarks after event selection criteria is denoted by $\varepsilon_{\text{hadron}}^b$ (for hadronic events) and $\varepsilon_{\text{tag}}^b$ (for double b -tagged events). Similarly, the averaged detection efficiency for light quarks ($q = u, d, s, c$) is denoted by $\varepsilon_{\text{hadron}}^{udsc}$ (for hadronic events) and $\varepsilon_{\text{tag}}^{udsc}$ (for double b -tagged events), weighted by the cross section of $e^+e^- \rightarrow q\bar{q}$. The values are $\varepsilon_{\text{hadron}}^{udsc} = 52.48\%$, $\varepsilon_{\text{hadron}}^b = 52.70\%$, $\varepsilon_{\text{tag}}^b = 46.42\%$, and $\varepsilon_{\text{tag}}^{udsc} = 0.04\%$ (End Matter). The correction factors f_{ISR}^{udsc} and f_{ISR}^b are used to model the effects of initial state radiation (ISR) and energy spread. Meanwhile, N_{tag} (N_{hadron}) is the number of selected double b -tagged hadronic events (the number of hadronic events) from the experiment datasets, and can be obtained with information of the cross section, integrated luminosity, and detection efficiency at an energy point. If we ignore the small values $\varepsilon_{\text{hadron}}^{udsc} - \varepsilon_{\text{hadron}}^b$, $\varepsilon_{\text{tag}}^{udsc}$, and $1 - f_{\text{ISR}}^b/f_{\text{ISR}}^{udsc}$, we can get $R_b \sim (N_{\text{tag}} \varepsilon_{\text{hadron}}^{udsc}) / (N_{\text{hadron}} \varepsilon_{\text{tag}}^b)$. Then the R_b value and its corresponding statistical uncertainty can be determined at an energy point (End Matter).

The chi-square statistic (χ^2) is a standard tool used to evaluate the significance of a signal or the goodness of fit of a given model. In pseudo-experiments, we perform an analysis on datasets generated by SM with J_t model to extract R_b value (R_b^{PEX}) at a chosen energy point (\sqrt{s}_i). The χ^2 is then defined as follows:

$$\chi_{\text{Model}}^2 = \sum_i \left(\frac{R_b^{\text{PEX}}(\mathcal{L}_i, \sqrt{s}_i) - R_b^{\text{Model}}(\mathcal{L}_i, \sqrt{s}_i)}{\Delta R_b^{\text{PEX}}(\mathcal{L}_i, \sqrt{s}_i)} \right)^2. \quad (8)$$

The \mathcal{L}_i is the integrated luminosity at \sqrt{s}_i , and $\Delta R_b^{\text{PEX}}(\mathcal{L}_i, \sqrt{s}_i)$ is the uncertainty of $R_b^{\text{PEX}}(\mathcal{L}_i, \sqrt{s}_i)$. The fitting function $R_b^{\text{Model}}(\mathcal{L}_i, \sqrt{s}_i)$ gives a theoretical R_b value at an energy point, where free parameters m_{J_t} and λ can be varied to minimize χ_{Model}^2 .

Three sets of energy points are selected as $\sqrt{s} = (340.076, 341.598, 342.771)$ GeV, and the corresponding luminosities are determined as $\mathcal{L} = (80, 300, 20)$ fb $^{-1}$, to make the significance of the J_t signal exceeding 5σ discussed below. With this statistical strategy, we can obtain the maximum values of χ_i^2/\mathcal{L}_i (or $\partial R_b/\partial \sqrt{s} = 0$) for the first and third energy points, and a χ_i^2/\mathcal{L}_i value close to zero (but $\partial R_b/\partial m_t$ is maximum) for the second point, used to measure the m_t^{IS} . This behavior is also well understood in the quantum interference picture, where the first and third energy points correspond to the minimum and maximum values of the interference, respectively, while the second energy

point is the point where the interference is nearly close to zero. The significance of the J_t signal is calculated by $\Delta\chi^2/\text{dof} = (\chi_{\text{SM without } J_t}^2 - \chi_{\text{SM with } J_t}^2)/\text{dof}$, where dof is the number of degrees of freedom. The values of R_b^{PEX} along with their respective statistical uncertainties are shown in Fig. 1. Considering only the statistical uncertainty, the significance of the J_t signal amounts to 6.26σ .

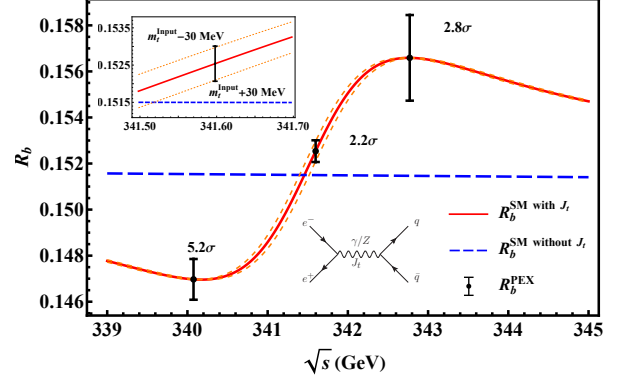


FIG. 1. The blue dashed line represents R_b distribution in SM without J_t , the red solid line represents R_b distribution in SM with J_t , and the statistical significance of the three energy points is indicated. The upper left insert shows R_b values for m_t^{Input} and $m_t^{\text{Input}} \pm 30$ MeV near the second energy point. The lower right insert shows the LO Feynman diagram for $e^+e^- \rightarrow q\bar{q}$, where the propagator can be a photon, a Z , or a J_t .

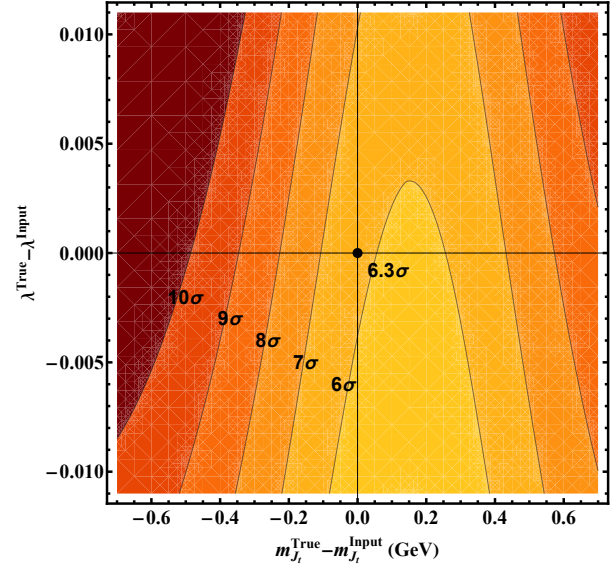


FIG. 2. Significance of the J_t signal varies with m_{J_t} and λ within the 1σ range.

The main sources of systematic uncertainties in the R_b measurements are the energy scale of \sqrt{s} , energy spread,

detection efficiency, and backgrounds. All systematic uncertainties are more than an order of magnitude smaller than the statistical uncertainties (End Matter), leading to a J_t signal significance of 6.25σ even when the total systematic uncertainties are taken into account.

When the true values of m_{J_t} and λ vary within their respective 1σ ranges, we determine the corresponding significance of the J_t signal. This significance consistently exceeds the 5σ threshold and is shown in Fig. 2.

Extracting m_t^{1S} —The top quark mass m_t^{1S} (along with the coefficient λ) is extracted by minimizing $\chi_{\text{SM with } J_t}^2$. The statistical uncertainty $(\Delta m_t^{1S})_{\text{stat.}}$ is found to be 32.2 MeV, primarily determined by the second energy point $\sqrt{s_2}$. The systematic uncertainties, $(\Delta m_t^{1S})_{\text{sys.}}$, arise from several sources, including the energy scale and energy spread, detection efficiency, SM parameters, higher order corrections, and others (luminosity measurements and backgrounds from two-photon and WWZ processes).

The uncertainty of $\sqrt{s_2}$ energy scale is estimated to be 2.0 MeV at $2m_t^{1S}$ [50], which directly enters into the m_{J_t} and contributes 1.0 MeV to Δm_t^{1S} . The center of mass energy spread is 458.4 MeV at $\sqrt{s_2}$ [14, 16], with an estimated uncertainty of 10% [16, 50], contributing an additional 0.2 MeV to Δm_t^{1S} .

Experimentally, the backgrounds, as well as the detection efficiency and the weak mixing angle θ_W , can be determined primarily by the data from Z , WW , and HZ peaks, which are directly translated to the m_{J_t} region [51]. The detection efficiency related uncertainty in R_b is $\varepsilon_{\text{hadron}}^{udsc} / \varepsilon_{\text{tag}}^b$, which is consistent that in the R_b measurement at the Z pole. After including uncertainties from Monte Carlo statistics and energy-momentum requirement, the uncertainty associated with the detection efficiency in R_b is 19.1×10^{-6} (End Matter). This is about half of the total uncertainty of the R_b measurement at the Z pole at CEPC, which is 4×10^{-5} [13]. Consequently, this contributes 1.3 MeV to Δm_t^{1S} .

By comparing the background contributions estimated in theory and observed in experiment, a relative precision of $(\alpha_s/\pi)^2 \sim 10^{-3}$ can be achieved, contributing 0.9 MeV to Δm_t^{1S} . Additionally, $\sin^2 \theta_W$ can attain an accuracy of 1×10^{-5} [13], thereby contributing 0.4 MeV to Δm_t^{1S} . The NNLO correction of R_b yields a contribution of 0.1 MeV to Δm_t^{1S} . The contribution of other sources, such as luminosity and backgrounds from two-photon and WWZ processes, is less than 0.2 MeV for Δm_t^{1S} (End Matter).

Assuming these sources are independent, we combine them in quadrature, yielding a total systematic uncertainty of $(\Delta m_t^{1S})_{\text{sys.}} = 1.9$ MeV, as summarized in Table I. Then we get:

$$\Delta m_t^{1S} = (\pm 32.2_{\text{stat.}} \pm 1.9_{\text{sys.}}) \text{ MeV} = \pm 32.3 \text{ MeV}. \quad (9)$$

The systematic uncertainty of our method is greatly

improved over the predictions of previous studies [16, 17] due to simpler final states and differences in the physical quantities to be measured. The final states in Refs. [16, 17] are six-body systems from $e^+e^- \rightarrow t\bar{t} \rightarrow b\bar{b}WW$, where W decays into quark pairs or lepton-neutrino pairs, while our method focuses on two-body final states $b\bar{b}$.

The upcoming e^+e^- colliders aim to achieve integrated luminosities of $1,000 \text{ fb}^{-1}$ at CEPC [14] and $1,700 \text{ fb}^{-1}$ at FCC-ee [15], respectively, near the $t\bar{t}$ production threshold. With these luminosities, the systematic uncertainty on m_t^{1S} is expected to remain at 1.9 MeV for both CEPC and FCC-ee. If the luminosities are chosen as $\mathcal{L} = (80, 900, 20) \text{ fb}^{-1}$ and $\mathcal{L} = (80, 1,600, 20) \text{ fb}^{-1}$ for CEPC and FCC-ee at (340.076, 341.598, 342.771) GeV, respectively, our results show that, the statistical uncertainty, $(\Delta m_t^{1S})_{\text{stat.}}$, is estimated to be 18.6 MeV for CEPC and 13.9 MeV for FCC-ee, or 11.2 MeV when data from both colliders are combined. A detailed comparison of the top quark mass measurement methods at CEPC [16], FCC-ee [17], and in this work is presented in Table II.

Discussion and Outlook—In this Letter, we propose a method for both discovering toponium and precisely measuring the top quark mass m_t^{1S} using the observable R_b near the energy threshold $2m_t^{1S}$ in e^+e^- collisions. The significance of the toponium signal exceeds 5σ , including both statistical and systematic uncertainties with the integrated luminosity of 400 fb^{-1} around 341 GeV. The m_t^{1S} can be measured with a total uncertainty of only 32.3 MeV, including a systematic uncertainty of 1.9 MeV. This enables a top quark mass measurement with an uncertainty reduced by a factor of 10 compared to the current precision [2]. Additionally, polarized beams or the well separation of b -jet and \bar{b} -jet in detection can reduce the integrated luminosities by an order of magnitude.

As the smallest quantum bound state and simplest hadron, toponium provides a unique opportunity to probe fundamental principles of quantum mechanics [3, 5], including particle-wave duality, entanglement, and spin dynamics, while offering novel insights into the nature of confinement in QCD [28]. A precise measurement of m_t is crucial in particle physics, as it directly impacts the stability of SM vacuum and determines whether the universe exists in a metastable state [11, 12].

Acknowledgments—We thank Profs. Kuang-Ta Chao, Gang Li, Yan-Qing Ma, Manqi Ruan, Xiaohu Sun, and Shi-Lin Zhu for valuable and helpful discussions. This work is supported in part by National Key Research and Development Program of China under Contract No. 2024YFA1610503, National Natural Science Foundation of China (NSFC) under contract No. 12161141008, No. 12135005, and No. 12405102, the Fundamental Research Funds for the Central Universities Grant No. 4007022302, and the China Postdoctoral Science Foundation under Grant No. 2024M750049.

TABLE I. Systematic uncertainties of the m_t measurement in MeV. The ‘‘Other’’ category includes luminosity measurements and backgrounds from two-photon and WWZ processes.

Δm_t (MeV)	FCC-ee [17]	CEPC [16]	This work
Energy scale	3	2	1.0
Energy spread	–	3 – 5	0.2
Efficiency	–	5 – 45	1.3
Background	10 – 20	4 – 18	0.9
SM parameters (θ_W, α_s)	3.2	17	0.4
Higher order corrections	40 – 45	9 – 26	0.1
Other	–	10	< 0.2
Total syst.	40 – 74	23 – 58	1.9

TABLE II. Detailed comparison of the top quark mass measurement methods: final states, signal and background cross sections, and uncertainty estimation at CEPC [16], FCC-ee [17], and in this work.

Method	CEPC [16]	FCC-ee [17]	This work
Final states	$b\bar{b}f\bar{f}f\bar{f}$	$b\bar{b}f\bar{f}f\bar{f}$	$b\bar{b}, q\bar{q}$
Measured quantity	$\sigma(t\bar{t})$	$\sigma(t\bar{t})$	$R_b = \sigma(b\bar{b})/\sigma(q\bar{q})$
σ_{signal}	$\sim 450 \text{ fb}$ [18]	$\sim 450 \text{ fb}$ [18]	$\sim 900 \text{ fb}$ ($b\bar{b}$), $\sim 6,000 \text{ fb}$ ($q\bar{q}$)
Signal over background	~ 2.9 [18]	~ 2.9 [18]	$\sim 89, \sim 12$
\sqrt{s} (GeV)	$\sim 343 \text{ GeV}$	$\sim 343 \text{ GeV}$	$\sim 341 \text{ GeV}$
Integrated luminosity	100 fb^{-1}	200 fb^{-1}	$400 - 2,700 \text{ fb}^{-1}$
$(\Delta m_t)_{\text{stat.}}$	9 MeV	9 MeV	11.2 – 32.2 MeV
$(\Delta m_t)_{\text{syst.}}$	23 – 58 MeV	40 – 74 MeV	1.9 MeV
$(\Delta m_t)_{\text{total}}$	25 – 59 MeV	45 – 75 MeV	11.3 – 32.3 MeV

- * These authors contributed equally to this work.
[†] zyj@buaa.edu.cn (Corresponding author)
[‡] shencp@fudan.edu.cn (Corresponding author)
- [1] V. M. Abazov *et al.* (DØ Collaboration), *Nature* **429**, 638 (2004), arXiv:hep-ex/0406031.
[2] A. Hayrapetyan *et al.* (CMS Collaboration, ATLAS Collaboration), *Phys. Rev. Lett.* **132**, 261902 (2024), arXiv:2402.08713 [hep-ex].
[3] F. Maltoni, C. Severi, S. Tentori, and E. Vryonidou, *JHEP* **09** (9), 001, arXiv:2404.08049 [hep-ph].
[4] G. Aad *et al.* (The ATLAS Collaboration), *Nature* **633**, 542 (2024), arXiv:2311.07288 [hep-ex].
[5] J. A. Aguilar-Saavedra and J. A. Casas, *Phys. Rev. Lett.* **133**, 111801 (2024), arXiv:2401.06854 [hep-ph].
[6] T. Han, M. Low, N. McGinnis, and S. Su, *Measuring Quantum Discord at the LHC* (2024), arXiv:2412.21158 [hep-ph].
[7] G. Domènech, M. Goodsell, and C. Wetterich, *JHEP* **01** (1), 180, arXiv:2008.04310 [hep-ph].
[8] G. F. Giudice, R. Rattazzi, and J. D. Wells, *Nucl. Phys. B* **544**, 3 (1999), arXiv:hep-ph/9811291.
[9] G. Aad *et al.* (The ATLAS Collaboration), *Nature* **607**, 52 (2022), [Erratum: *Nature* **612**, E24 (2022)], arXiv:2207.00092 [hep-ex].
[10] A. Tumasyan *et al.* (The CMS Collaboration), *Nature* **607**, 60 (2022), [Erratum: *Nature* **623**, E4 (2023)], arXiv:2207.00043 [hep-ex].
[11] S. Alekhin, A. Djouadi, and S. Moch, *Phys. Lett. B* **716**, 214 (2012), arXiv:1207.0980 [hep-ph].
[12] V. Branchina, E. Messina, and M. Sher, *Phys. Rev. D* **91**, 013003 (2015), arXiv:1408.5302 [hep-ph].
[13] M. Dong *et al.* (The CEPC Study Group), CEPC Conceptual Design Report: Volume 2 - Physics & Detector (2018), arXiv:1811.10545 [hep-ex].
[14] W. Abdallah *et al.*, *Radiat. Detect. Technol. Methods* **8**, 1 (2024), arXiv:2312.14363 [physics.acc-ph].
[15] A. Abada *et al.*, *Eur. Phys. J. ST* **228**, 261 (2019).
[16] Z. Li, X. Sun, Y. Fang, G. Li, S. Xin, S. Wang, Y. Wang, Y. Zhang, H. Zhang, and Z. Liang, *Eur. Phys. J. C* **83**, 269 (2023), [Erratum: *Eur. Phys. J. C* **83**, 501 (2023)], arXiv:2207.12177 [hep-ex].
[17] R. Schwienhorst *et al.*, Report of the Topical Group on Top quark physics and heavy flavor production for Snowmass 2021 (2022), arXiv:2209.11267 [hep-ph].
[18] K. Seidel, F. Simon, M. Tesař, and S. Poss, *Eur. Phys. J. C* **73**, 2530 (2013), arXiv:1303.3758 [hep-ex].
[19] L. J. Hall, R. Rattazzi, and U. Sarid, *Phys. Rev. D* **50**, 7048 (1994), arXiv:hep-ph/9306309.
[20] A. Denner, R. J. Guth, and J. H. Kühn, *Phys. Lett. B* **240**, 438 (1990).
[21] D. Rodriguez Roman and M. Fairbairn, *Phys. Rev. D* **99**, 036012 (2019), arXiv:1807.02450 [hep-ph].
[22] I. Masina and A. Notari, *Phys. Rev. Lett.* **108**, 191302 (2012), arXiv:1112.5430 [hep-ph].
[23] A. Eichhorn and A. Held, *Phys. Lett. B* **777**, 217 (2018), arXiv:1707.01107 [hep-th].
[24] A. H. Hoang and M. Stahlhofen, *JHEP* **05** (5), 121, arXiv:1309.6323 [hep-ph].
[25] P. Marquard, A. V. Smirnov, V. A. Smirnov, M. Stein-

- hauser, and D. Wellmann, *Phys. Rev. D* **94**, 074025 (2016), arXiv:1606.06754 [hep-ph].
- [26] G. Corcella, *Front. in Phys.* **7**, 54 (2019), arXiv:1903.06574 [hep-ph].
- [27] A. H. Hoang, *Ann. Rev. Nucl. Part. Sci.* **70**, 225 (2020), arXiv:2004.12915 [hep-ph].
- [28] M. R. Shepherd, J. J. Dudek, and R. E. Mitchell, *Nature* **534**, 487 (2016), arXiv:1802.08131 [hep-ph].
- [29] R. D. Ball, A. Candido, J. Cruz-Martinez, S. Forte, T. Giani, F. Hekhorn, K. Kudashkin, G. Magni, and J. Rojo (The NNPDF Collaboration), *Nature* **608**, 483 (2022), arXiv:2208.08372 [hep-ph].
- [30] L. Apolinário, J. G. Milhano, G. P. Salam, and C. A. Salgado, *Phys. Rev. Lett.* **120**, 232301 (2018), arXiv:1711.03105 [hep-ph].
- [31] E. Suhonen, *Phys. Lett. B* **119**, 81 (1982).
- [32] E. Witten, *Nucl. Phys. B* **177**, 477 (1981).
- [33] Y. Guan and S. Matsuzaki, *JHEP* **09** (9), 140, arXiv:2405.03265 [hep-ph].
- [34] W. Liu and K.-P. Xie, *Phys. Rev. D* **110**, 115001 (2024), arXiv:2408.03649 [hep-ph].
- [35] A. Blondel and P. Janot, *Eur. Phys. J. Plus* **137**, 92 (2022), arXiv:2106.13885 [hep-ex].
- [36] A. Greljo, H. Tiplom, and A. Valenti, *New Physics Through Flavor Tagging at FCC-ee* (2024), arXiv:2411.02485 [hep-ph].
- [37] B. Fuks, K. Hagiwara, K. Ma, and Y.-J. Zheng, *Phys. Rev. D* **104**, 034023 (2021), arXiv:2102.11281 [hep-ph].
- [38] J. A. Aguilar-Saavedra, *Phys. Rev. D* **110**, 054032 (2024), arXiv:2407.20330 [hep-ph].
- [39] S.-J. Jiang, B.-Q. Li, G.-Z. Xu, and K.-Y. Liu, *Study on toponium: Spectrum and associated processes* (2024), arXiv:2412.18527 [hep-ph].
- [40] G. T. Bodwin, E. Braaten, and G. P. Lepage, *Phys. Rev. D* **51**, 1125 (1995), [Erratum: *Phys. Rev. D* **55**, 5853 (1997)], arXiv:hep-ph/9407339.
- [41] T. Kawanai and S. Sasaki, *Phys. Rev. D* **89**, 054507 (2014), arXiv:1311.1253 [hep-lat].
- [42] Y. Koma and M. Koma, *Nucl. Phys. B* **769**, 79 (2007), arXiv:hep-lat/0609078.
- [43] M. Beneke, A. Maier, J. Piclum, and T. Rauh, *Nucl. Phys. B* **899**, 180 (2015), arXiv:1506.06865 [hep-ph].
- [44] L. Jeppe, *Search for heavy scalar or pseudoscalar states in $t\bar{t}$ events at CMS* (2024), arXiv:2411.18414 [hep-ex].
- [45] L. Chen, X. Chen, X. Guan, and Y.-Q. Ma, *Top-Quark Decay at Next-to-Next-to-Next-to-Leading Order in QCD* (2023), arXiv:2309.01937 [hep-ph].
- [46] L.-B. Chen, H. T. Li, Z. Li, J. Wang, Y. Wang, and Q.-F. Wu, *Phys. Rev. D* **109**, L071503 (2024), arXiv:2309.00762 [hep-ph].
- [47] H. Überall, *Phys. Rev.* **119**, 365 (1960).
- [48] J.-H. Fu, S. Jia, X.-Y. Zhou, Y.-J. Zhang, C.-P. Shen, and C.-Z. Yuan, *Sci. Bull.* **69**, 1386 (2024), arXiv:2305.00171 [hep-ph].
- [49] S. Schael *et al.* (The ALEPH Collaboration), *Eur. Phys. J. C* **49**, 411 (2007), arXiv:hep-ex/0609051.
- [50] A. Blondel *et al.*, *Polarization and Centre-of-mass Energy Calibration at FCC-ee* (2019), arXiv:1909.12245 [physics.acc-ph].
- [51] R. Barate *et al.* (The ALEPH Collaboration), *Eur. Phys. J. C* **12**, 183 (2000), arXiv:hep-ex/9904011.
- [52] M. Beneke, Y. Kiyo, and K. Schuller, *Nucl. Phys. B* **714**, 67 (2005), arXiv:hep-ph/0501289.
- [53] M. Beneke, Y. Kiyo, A. Maier, and J. Piclum, *Comput. Phys. Commun.* **209**, 96 (2016), arXiv:1605.03010 [hep-ph].
- [54] M. Beneke, A. Maier, T. Rauh, and P. Ruiz-Femenía, *JHEP* **02** (2), 125, arXiv:1711.10429 [hep-ph].
- [55] M. Beneke and Y. Kiyo, *Third-order correction to top-quark pair production near threshold II. Potential contributions* (2024), arXiv:2409.05960 [hep-ph].
- [56] S. Navas *et al.* (Particle Data Group), *Phys. Rev. D* **110**, 030001 (2024).
- [57] A. Blondel, J. Gluza, S. Jadach, P. Janot, and T. Riemann, eds., *Theory for the FCC-ee: Report on the 11th FCC-ee Workshop Theory and Experiments*, CERN Yellow Reports: Monographs, Vol. 3/2020 (CERN, Geneva, 2019) arXiv:1905.05078 [hep-ph].
- [58] F. Herren and M. Steinhauser, *Comput. Phys. Commun.* **224**, 333 (2018), arXiv:1703.03751 [hep-ph].
- [59] E. A. Kuraev and V. S. Fadin, *Sov. J. Nucl. Phys.* **41**, 466 (1985).
- [60] P. Ruiz-Femenía and A. Pich, *Phys. Rev. D* **64**, 053001 (2001), arXiv:hep-ph/0103259.
- [61] A. Djouadi, J. H. Kühn, and P. M. Zerwas, *Z. Phys. C* **46**, 411 (1990).
- [62] K. G. Chetyrkin, R. Harlander, J. H. Kühn, and M. Steinhauser, *Nucl. Phys. B* **503**, 339 (1997), arXiv:hep-ph/9704222.
- [63] V. A. Novikov, L. B. Okun, A. N. Rozanov, and M. I. Vysotsky, *Rept. Prog. Phys.* **62**, 1275 (1999), arXiv:hep-ph/9906465.
- [64] X. Chen, X. Guan, C.-Q. He, X. Liu, and Y.-Q. Ma, *Phys. Rev. Lett.* **132**, 101901 (2024), arXiv:2209.14259 [hep-ph].
- [65] K. G. Chetyrkin, R. V. Harlander, and J. H. Kühn, *Nucl. Phys. B* **586**, 56 (2000), [Erratum: *Nucl. Phys. B* **634**, 413–414 (2002)], arXiv:hep-ph/0005139.
- [66] W. Kilian, T. Ohl, and J. Reuter, *Eur. Phys. J. C* **71**, 1742 (2011), arXiv:0708.4233 [hep-ph].
- [67] T. Sjöstrand, S. Mrenna, and P. Z. Skands, *JHEP* **05** (05), 026, arXiv:hep-ph/0603175.
- [68] J. de Favereau, C. Delaere, P. Demin, A. Giammanco, V. Lemaitre, A. Mertens, and M. Selvaggi (The DELPHES 3 Collaboration), *JHEP* **02** (2), 057, arXiv:1307.6346 [hep-ex].
- [69] M. Cacciari, G. P. Salam, and G. Soyez, *JHEP* **04** (04), 063, arXiv:0802.1189 [hep-ph].
- [70] G. Alexander *et al.* (OPAL Collaboration), *Phys. Lett. B* **376**, 232 (1996).
- [71] Z. Wu, G. Li, D. Yu, C. Fu, Q. Ouyang, and M. Ruan, *JINST* **13** (09), T09002.
- [72] P.-Z. Lai, M. Ruan, and C.-M. Kuo, *JINST* **16** (07), P07037, arXiv:2104.05029 [hep-ex].

End Matter

Theoretical calculation—The binding energy B_J can also be calculated in perturbative QCD (PQCD), yielding $(1.57_{\text{LO}} + 0.65_{\text{NLO}} + 0.49_{\text{NNLO}} + 0.25_{\text{NNNLO}}) \text{ GeV} = 2.96$

GeV at NNNLO with a renormalization scale of $\mu = 32.6$ GeV for m_{J_t} and $\mu = 30$ GeV for m_t^{OS} [52]. The difference between m_t^{OS} and m_t^{IS} is calculated to be $(0.428_{\text{LO}} + 0.368_{\text{NLO}} + 0.262_{\text{NNLO}} + (0.174 \pm 0.0004)_{\text{NNNLO}})$ GeV = (1.232 ± 0.0004) GeV at NNNLO with $\mu = 163.508$ GeV [25]. With the center value of $m_t^{\text{OS}} = 172.52$ GeV [2], the `QQbar_threshold` package [53–55] yields:

$$B_{J_t}^{\text{PQCD}} = (1.680_{\text{LO}} + 0.657_{\text{NLO}} + 0.504_{\text{NNLO}} + 0.243_{\text{NNNLO}}) \text{ GeV} = 3.084 \text{ GeV} \quad (10)$$

at NNNLO with $\mu = 1/r_B = 24.584$ GeV, where r_B is the Bohr radius. However, the convergence of the perturbative series up to NNNLO is still unsatisfactory, necessitating consideration of higher order corrections.

The running parameters are chosen at the energy scale of m_{J_t} for both theoretical calculations and experimental simulations [2, 56–58]:

$$\begin{aligned} m_b &= 2.568(10) \text{ GeV} \quad , \quad m_c = 0.575(3) \text{ GeV}, \\ m_H &= 125.20(11) \text{ GeV} \quad , \quad \alpha_s = 0.09844(62), \\ m_Z &= 91.1880(20) \text{ GeV} \quad , \quad \alpha = 1/126.04(1), \\ m_W &= 80.3692(133) \text{ GeV} \quad , \quad \cos \theta_W = m_W/m_Z. \end{aligned} \quad (11)$$

The experimental cross section, denoted by the symbol σ , is given by the following expression [48, 54]:

$$\begin{aligned} \sigma(\sqrt{s}, \delta_{\sqrt{s}}) &= \int d\sqrt{s'} \frac{1}{\sqrt{2\pi}\delta_{\sqrt{s}}} e^{-\frac{(\sqrt{s}-\sqrt{s'})^2}{2\delta_{\sqrt{s}}^2}} \\ &\times \int dx F(x, \sqrt{s'}) \bar{\sigma}(\sqrt{x s'}) = f_{\text{ISR}} \sigma_{\text{Born}}. \end{aligned} \quad (12)$$

In this formula, $\delta_{\sqrt{s}}$ is the center of mass energy spread, and the ISR factor $F(x, \sqrt{s'})$ is given in Refs. [54, 59, 60]. Then, we can obtain f_{ISR} , the factor that includes the effects of energy spread and ISR.

In SM, the LO [56], NLO [61], NNLO [62] and NNNLO [63–65] predictions of R_b at \sqrt{s} around m_{J_t} are:

$$\begin{aligned} R_b^{\text{SM}} &= \left[151,550.2_{\text{LO}} - 50.6_{\text{NLO}} + 0.8_{\text{NNLO}} \right. \\ &\quad \left. + 0.0_{\text{NNNLO}} - 27.4 \times \frac{\sqrt{s} - m_{J_t}}{\text{GeV}} \right. \\ &\quad \left. + 0.1 \times \left(\frac{\sqrt{s} - m_{J_t}}{\text{GeV}} \right)^2 + \dots \right] \times 10^{-6}. \end{aligned} \quad (13)$$

The $R_b(\sqrt{s_i})$ is determined by the cross sections of $\sigma(e^+e^- \rightarrow b\bar{b})$ and $\sigma(e^+e^- \rightarrow q\bar{q})$ at the selected $\sqrt{s_i}$:

$$\begin{aligned} N_{\text{tag}}(\sqrt{s_i}) &= \mathcal{L}_i \sum_{q=uds cb} \varepsilon_{\text{tag}}^q \sigma(e^+e^- \rightarrow q\bar{q}), \\ N_{\text{hadron}}(\sqrt{s_i}) &= \mathcal{L}_i \sum_{q=uds cb} \varepsilon_{\text{hadron}}^q \sigma(e^+e^- \rightarrow q\bar{q}) \end{aligned} \quad (14)$$

The N_{tag} , N_{hadron} , $\varepsilon_{\text{tag}}^q$, and $\varepsilon_{\text{hadron}}^q$ are defined after Eq.(7). Then the R_b is defined in Eq.(7).

Experimental simulation—In this Letter, MC simulations of e^+e^- collisions have been performed. The physics events are generated using `Whizard` [66], where the effects of ISR and energy spread have been taken into account. Subsequently, `Pythia6` [67] is applied for parton showering, hadronization, and the decay processes of the short-life hadrons. Finally, `Delphes` [68], configured with the CEPC detector conditions [13], is used to simulate the detector response. To measure R_b , samples with 2 fermions ($u\bar{u}, d\bar{d}, s\bar{s}, c\bar{c}, b\bar{b}$) are generated. Moreover, due to limitations in detector performance, some jets with low energy or those produced at extreme angles relative to the detector’s central axis [13, 15] may go undetected. To address this, several multi-jet backgrounds from WW , ZZ , and ZH decays to four-quark final states are simulated. In order to enhance the sensitivity for J_t signal, the event selection criteria are optimized as discussed below.

Jets from $q\bar{q}$ are clustered from all the well reconstructed tracks with an anti-kt algorithm [69]. To select high-quality jets, we require jet transverse momentum (p_t) greater than 15 GeV. To include the case of gluon final state radiation in $q\bar{q}$ final state, the selected events are supposed to have 2 or 3 jets. As the detector does not cover all directions, the ISR photons and jets close to the beam direction may escape detection. Thus, the effective invariant mass of the final states $\sqrt{s'}$ needs to be considered. We require $\sqrt{s'} > \sqrt{s} - 10$ GeV here [49, 54, 70]. For the measurement of R_b , only events with at least two b -tagged jets [71] are categorized as $b\bar{b}$ events, while the remaining events are considered as light quark pair processes. For the selected signal events, we require the invariant mass of jet pairs M_{bb} or $M_{j_1 j_2}$ greater than 150 GeV to suppress the backgrounds from W/Z hadronic decays, where $j_1 j_2$ denote the two jets with the highest and the second-highest energies. Events passing all of the criteria are recognized as signal events, and the detection efficiencies of different processes in the three energy points are shown in Table III.

Systematic uncertainties—The systematic uncertainties, affecting the accuracy of R_b measurements, arise from accelerator effects (e.g., \sqrt{s} energy scale and energy spread), detector efficiencies (e.g., MC statistics, $\sqrt{s'}$ and p_t requirements), SM parameters (θ_W , α_s , etc.), theoretical considerations (e.g., higher order corrections and ISR), and others (e.g., luminosity measurements and backgrounds from two-photon and WWZ processes). Taking the R_b measurement at the second energy point as an example, systematic uncertainties are discussed below. The uncertainty in the energy scale of $\sqrt{s_2}$ is estimated to be 2 MeV [50], contributing 14.6×10^{-6} to ΔR_b . The energy spread at the second energy point is 458.4 MeV for CEPC, with a 10% uncertainty [16, 50] contributing

an additional 2.7×10^{-6} to ΔR_b . By increasing the size of simulated events, the statistical error can be reduced to less than 10^{-4} , resulting in a contribution of 15.4×10^{-6} to ΔR_b . The precisions of p_t and $\sqrt{s'}$ are controlled to within 0.10 GeV and 0.34 GeV [49, 72], respectively, leading to ΔR_b values of 9.1×10^{-6} and 6.7×10^{-6} . The WW , ZZ , and ZH related processes are well understood both theoretically and experimentally, with approximately 95% of such events rejected by selection criteria. The relative uncertainty in these backgrounds is less than $(\alpha_s/\pi)^2 \sim 0.001$, contributing 13.9×10^{-6} to

ΔR_b . The uncertainty in $\sin^2 \theta_W$, achievable at 1×10^{-5} at CEPC [13, 50], contributes 6.0×10^{-6} to ΔR_b . The uncertainty of m_b in Eq.(11) contributes 0.2×10^{-6} to ΔR_b , while the uncertainty from α_s is included in higher-order corrections. As shown in Eq.(13), the NNLO corrections increase R_b by 1.2×10^{-6} . The other sources include luminosity measurements and backgrounds from two-photon and WWZ processes. Their contributions to ΔR_b are small, with a combined estimation of less than 3.0×10^{-6} . All the systematic uncertainties are summarized in Table IV.

TABLE III. The experimental cross sections $\sigma(\sqrt{s})$ (in fb), along with the detection efficiencies ε_{tag} (in %, for double b -tagged events) and $\varepsilon_{\text{hadron}}$ (in %, for hadronic events), are provided for various processes in the R_b measurements. Here, jj denotes $u\bar{u}$, $d\bar{d}$, $s\bar{s}$, $c\bar{c}$, or $g\bar{g}$.

Process	$\sigma(340.076)$ (fb)	$\sigma(341.598)$ (fb)	$\sigma(342.771)$ (fb)	$\varepsilon_{\text{tag}}(\%)$	$\varepsilon_{\text{hadron}}(\%)$
$b\bar{b}$	866.99	880.50	896.87	46.42	52.70
jj	4,977.58	4,945.68	4,927.87	0.04	52.48
$ZZ/ZH \rightarrow b\bar{b}b\bar{b}$	16.17/12.14	16.01/11.88	15.86/11.70	0.31	0.31
$ZZ/ZH \rightarrow b\bar{b}jj$	116.42/46.06	115.11/45.11	114.19/44.42	1.64	2.21
$ZZ/ZH/WW \rightarrow jjjj$	209.21/8.60/5,263.55	207.11/8.42/5,202.29	205.38/8.29/5,157.25	0.00	5.19

TABLE IV. Uncertainties of R_b^{PEX} are given in a unit of 10^{-6} . The ‘‘Other’’ category includes luminosity measurements and backgrounds from two-photon and WWZ processes.

Source	340.076 GeV	341.598 GeV	342.771 GeV
Energy scale	0.5	14.6	0.1
Energy spread	36.0	2.7	58.9
MC statistics	14.8	15.4	15.8
p_t requirement	8.9	9.1	9.3
$\sqrt{s'}$ requirement	6.4	6.7	7.0
Backgrounds	13.5	13.9	14.2
SM parameters	5.0	6.0	6.8
Higher order corrections	1.2	1.2	1.2
Other	3.0	3.0	3.0
Sum of syst.	43.0	28.6	64.0
Stat.	884.4	471.2	1,859.3
Total	885.5	472.1	1,860.4